

On the thermalization of the three-dimensional, incompressible, Galerkin-truncated Euler equation

Sugan Durai Murugan^{*} and Samriddhi Sankar Ray[†]

International Centre for Theoretical Sciences, Tata Institute of Fundamental Research, Bangalore 560089, India

The long-time solutions of the Galerkin-truncated three-dimensional, incompressible Euler equation relax to an absolute equilibrium as a consequence of phase space and kinetic energy conservation in such a finite-dimensional system. These thermalized solutions are characterised by a Gibbs distribution of the velocity field and kinetic energy equipartition amongst its (finite) Fourier modes. We now show, through detailed numerical simulations, the triggers for the inevitable thermalization in physical space and how the problem is reducible to an effective one-dimensional problem making comparisons with the more studied Burgers equation feasible. We also discuss how our understanding of the mechanism of thermalization can be exploited to numerically obtain dissipative solutions of the Euler equations and evidence for or against finite-time blow-up in computer simulations.

Inviscid equations of hydrodynamics which are constrained to have a finite number of Fourier modes leads to thermalized flows which are distinctly different from our more accustomed viscous fluids. This is because Liouville's theorem ensures that the projection of the inviscid equations on a finite set of Fourier modes leads to, at long times, an inevitable thermalized, absolute equilibrium Gibbs state [1–4]. Consequently, this is accompanied by an equipartition of kinetic energy across Fourier modes \vec{k} [5–7] quite unlike the celebrated Kolmogorov scaling $\sim k^{-5/3}$ associated with turbulence in three dimensions (3D) or the k^{-2} scaling of the entropy solution in the one-dimensional (1D) Burgers problem [8]. Therefore such thermalized fluids are amenable to well-established theories of equilibrium statistical physics while being intrinsically chaotic. Recently, such nonlinear Hamiltonian systems have been used to settle questions in many-body statistical physics of ergodicity and mixing [9] as well as, admittedly in 1D, understanding vexing questions of complex-time singularities [10].

From the more specific vantage point of turbulence and fluid dynamics, the relevance of such systems is more subtle and less immediately obvious. This is particularly so for 3D turbulence where several fundamental questions remain unanswered. Hence, in the absence of the many theoretical tools available for studying the 1D Burgers equation [11], it is tempting to exploit the advantages of a 3D Galerkin-truncated incompressible Euler equation to make sense of real turbulent flows. Of course, superficially, such equilibrium solutions are in stark contrast to those obtained in (driven-dissipative) turbulence or in numerical solutions of the viscous Navier-Stokes equation. And yet the truncated equation retain the same nonlinear triadic structure as the parent inviscid partial differential equations or indeed, in three dimensions, the viscous Navier-Stokes equation which model turbulent flows. Thus in many ways the 3D Galerkin-truncated incompressible Euler equation is a compelling link between ideas of statistical physics for a Hamilto-

nian system with conserved dynamics [12, 13] and those which describe the behavior of out-of-equilibrium, driven-dissipative, viscous turbulent flows [14–16]. In the last couple of decades or so, since the work of L'vov *et al.* [17] and subsequently Frisch *et al.* [18], the generalisation of the idea of Galerkin truncation to fine-tune triadic interactions has lead to a narrowing of the gap between equilibrium statistical physics and turbulence. This, in particular, has been used most importantly in deepening of our understanding of central questions in 3D turbulence such as intermittency [19–25] and the issue of bottlenecks in the energy spectrum [26–28]. Most recently, the possibilities of small-scale thermalization in real flows [29] provides further impetus to studying the interplay of equilibrium statistical physics and turbulence often in dimensions which are not necessarily integer [30, 31].

There is another important reason why the Galerkin-truncated equation merits attention. One of the outstanding questions at the interface of physics and mathematics is the existence of weak or dissipative solutions [32, 33] and the possibility of finite-time blow-up for the 3D Euler equation [34–36]. While a review of this subject goes well beyond the scope of the present paper, suffice to say that probing the blow-up problem numerically is a monumental challenge [5, 37–59]. Indeed, conjectures remain speculative at best despite well-formulated criterion [60–67] which, in principle, should be easily detectable in well-resolved direct numerical simulations (DNSs) [68]. The obstacle to this however is that simulations are necessarily finite-dimensional: The commonly used spectral simulations [69, 70] solve the Galerkin-truncated and *not* the infinite-dimensional partial differential equations of inviscid flows. Hence, in finite times, which may well precede the time of blow-up (as is for the inviscid one-dimensional Burgers equation [71, 72]), the solutions thermalize (starting with the smallest scales) making methods for singularity-detection, such as the analyticity strip approach [73], arduous [59, 74]. Hence for finite

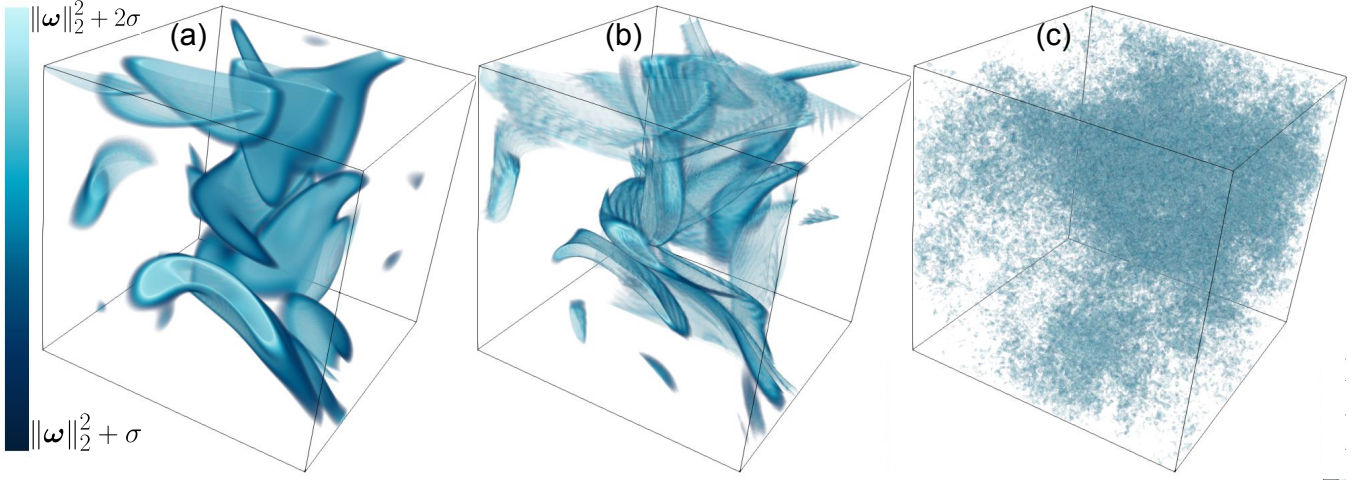


Figure 1. Isosurfaces of the vorticity field for $\sigma \leq |\omega|^2 - \|\omega\|_2^2 \leq 2\sigma$ at (a) $t = 0.5$, (b) $t = 0.85$ and (c) $t = 2.5$. See [here](#) for an animation of the evolution of these isosurfaces from a non-thermalized to a fully thermalized state.

resolutions, in the absence of convergence of such truncated solutions (which thermalize) to the actual (weak) solutions of the Euler equations themselves, conjectures on blow-ups from DNSs [60, 62, 67] will remain unsettled till mechanisms to circumvent Gibbs states in mathematically self-consistent ways are discovered. The discovery of such methods is of course contingent on knowing how truncated equations thermalize in the first place. It is useful to recall that such methods have been discovered for the more academic 1D Burgers problem [10, 75–78] owing to our thorough understanding of how the one-dimensional equation thermalizes.

Thus the long-time chaotic, Gibbs solutions [9] of the Galerkin-truncated Euler equations play contrasting roles in studies of fundamental problems in turbulence. On one hand, they allow us to connect ideas from statistical physics to turbulence and on the other they remain a stumbling block in numerical methods for studying questions of blow-up and dissipative solutions. This makes the understanding of how such 3D flows thermalize particularly essential. As a result in recent years, since the pioneering work of Cichowlas *et al.* [5], a reasonably complete picture of how energy equipartition happens in Fourier space has emerged [6, 7, 79, 80]. However, unlike the case of the 1D Burgers equation [71, 72, 75, 81], not much is known of the origins of thermalization in physical space for the 3D problem.

With this in mind, we perform detailed DNSs of the unit density Galerkin-truncated incompressible 3D Euler equation (Appendix A); the low-pass Galerkin projector \mathbb{P}_{k_G} ensures that Fourier modes of the velocity field are set to zero, via $\mathbb{P}_{k_G} \mathbf{u}(\mathbf{x}) = \sum_{|\mathbf{k}| \leq k_G} e^{i\mathbf{k} \cdot \mathbf{x}} \hat{\mathbf{u}}_{\mathbf{k}}$, for wavenumbers greater than a chosen threshold Galerkin-truncation wavenumber k_G .

While a long-time thermalized fluid, through Li-

ouville’s theorem, with Gibbs statistics [9] is obvious, the transition from a smooth initial condition which behaves like a “viscous” fluid for finite times to one which is thermalized and essentially devoid of structure, is far from obvious. A clue may be found in plots of the isosurfaces of the vorticity fields as they evolve in time. In Fig. 1(a) we show a plot of the vorticity ($\omega = \nabla \times \mathbf{u}$) isosurface for $\sigma \leq |\omega|^2 - \|\omega\|_2^2 \leq 2\sigma$, where σ is the standard deviation of the enstrophy field, at early times ($t = 0.5$) when the largest available wavenumbers are still not fully excited. When seen in the energy spectrum (Appendix A; Fig. A1) at the same time, there is no sign of thermalization. These enstrophy isosurfaces are smooth and indistinguishable from what one would expect from an extremely high Reynolds number Navier-Stokes simulations with similar initial conditions and at similar times. At slightly later times, ($t \gtrsim 0.85$) however isosurfaces show minute but detectable oscillatory structures Fig. 1(b) with wavelengths $\lambda_G = 2\pi/k_G$, reminiscent of what is seen for the corresponding problem in the one-dimensional Burgers equation [71, 72, 82]. We recall that a similar phenomenon was seen recently in simulations of the 3D, Galerkin-truncated *axisymmetric* incompressible Euler equation [59]. These initially localised (in both physical and Fourier space) oscillations rapidly spread through the domain, with increasing amplitudes, whilst becoming non-monochromatic. A snapshot of these fully thermalized states (Fig. 1(c)) looks noisy [78] with no resemblance to the well-formed isosurfaces which characterise fully-developed turbulence or indeed solutions of the truncated equation before the onset of thermalization (Fig. 1(a)). Consequently, the energy spectrum at such times and beyond converges to an equipartition $E(k) \sim k^2$ (Appendix A; also [5]).

While the signatures of thermalization are fairly obvious in plots such as those shown in Fig. 1, the incipient

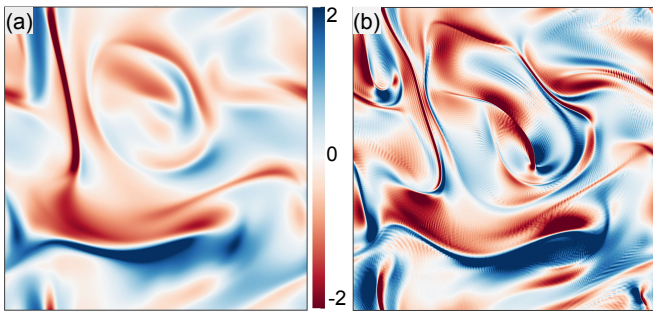


Figure 2. Pseudo-color plots of the strain field component S_{yz} in the XY plane at times (a) before ($t = 1.2$) and (b) after ($t = 1.8$) thermalization is triggered in the flow. While oscillatory structures are conspicuous by their absence for the former, coherent streaks of oscillations with wavelengths λ_G are clearly visible for the latter. See [here](#) for an animation of the evolution of S_{yz} from a non-thermalized to a fully thermalized state.

thermalized phase is best captured in visualisations of the velocity gradient. In Fig 2 we show two-dimensional (XY plane) cuts of the strain field $S_{ij} \equiv \partial u_i / \partial x_j$ which, at times when the effects of truncation are felt, show clear, organised oscillatory structures (panel (b)) which are absent at earlier times (panel (a)). We recall that in the one-dimensional (1D) inviscid Galerkin-truncated Burgers problem, the oscillatory structures that trigger thermalization are initially localised at point(s) co-moving with the shock(s) through a resonance effect [71]. The flow we study now is fundamentally different: It is three-dimensional and incompressible. So how does thermalization kick in (Figs. 1(b) and 2(b)) the 3D Euler equations and is there an analogue of resonance points or do the oscillations appear *out of the blue*?

The answer to this is delicate and Fig. 2(b) is suggestive. Starting from initial conditions (such as the ones we have) which concentrates energy at large scales, the nonlinearity of the systems generates smaller and smaller scales in time and generates structures ranging from of vortex sheets to tubes. As smaller and smaller scales get excited, many of these structures can sharpen (as thin sheets or tubes) [51, 54, 83] with a characteristic length scale $\sim k_G^{-1}$. Such sharp structures, analogous to shocks in the 1D Burgers equation, act as a source of *truncation waves* of wavelength λ_G —indeed the Fourier transform of the projection operator is a wave with wavenumber k_G —which travel along the directions in which such structures are compressed. In the representative snapshot shown in Fig. 2(b) the oscillations appear with wave vectors which, for this realization of the flow, are clearly normal to the intense structures seen in the domain. Of course, whether such oscillations amplify or rapidly diminish in space and time is determined by the nature of the strain field locally as we illustrate below. For oscillations which do survive, the nonlinearity allows other modes to get quickly ex-

cited and the nonlocality of the incompressible equation allows a rapid spread of these complex oscillations across the whole domain. This eventually leads to a chaotic, thermalized fluid, bereft of structure, and equipartition of kinetic energy across Fourier modes as illustrated in Fig. 1(c).

This phenomenological picture, though compelling, is difficult to *prove* in numerical simulations with the generic initial conditions that we use: The complexity of the spatial structures generated does not allow an easy way to test the different ingredients which go into the argument constructed above. In order to substantiate our theory, we resort to DNSs which are controlled in a way to isolate the two different effects at play: The sharpening of velocity gradients $\nabla u \sim 1/k_G$ and the consequent onset of thermalization along specific direction(s) relative to such intense structures.

Amongst the many candidate flows—such as isolated vortex tubes and sheets—we choose to work with an initial condition consisting of two separated, oppositely-signed vortex sheets (in the YZ plane), located symmetrically at $x = x_1$ and $x = -x_1$, in a periodic box $[-\pi, \pi]^3$. Furthermore, these sheets have a localised perturbing flow at their centers to disturb the sheet from equilibrium (Appendix B; Eq. (B1)). This flow field, with the large scale background flow (which creates the sheet) suppressed (for clarity), is illustrated in Fig. 3(a) along with the two-dimensional velocity vectors which illustrate the regions of compression.

By using Fig. 3(a) as initial conditions, we solve the Galerkin-truncated equation with $k_G = N/3$. Given the specific configuration that we chose, the centers of both the sheets start to develop sharper gradients: Along the compressional directions, at an angle $\pi/6$ at $-\mathbf{x}_1$ and $\pi/3$ at \mathbf{x}_1 away from the horizontal (indicated in Fig. 3(a) by blue and red dashed lines, respectively), the perturbations lead to a squeezing of the vortex sheet. As a result, these structures sharpen and eventually the gradients become comparable to the inverse of the truncation wavenumber. Thus, truncation waves are born as explained before.

In the analogous, 1D Burgers problem these truncation waves emerge from the region of the pre-shock and are constrained to travel along the one-dimensional velocity field. Therefore, in the Burgers problem, it is straightforward to identify the location of the oscillations: They ride on top of the one-dimensional velocity field. But for three-dimensional flows such as ours, there are infinitely many possible directions along which these oscillations emerge. Indeed, if such directions are chosen randomly by the truncated dynamics, then the problem of thermalization and, crucially, finding ways to circumvent becomes exceptionally hard. Fortunately, as we show below, the solution to this is simpler and can be mapped to an effective one-dimensional problem as we show below.

Given these are three-dimensional flows, it is reason-

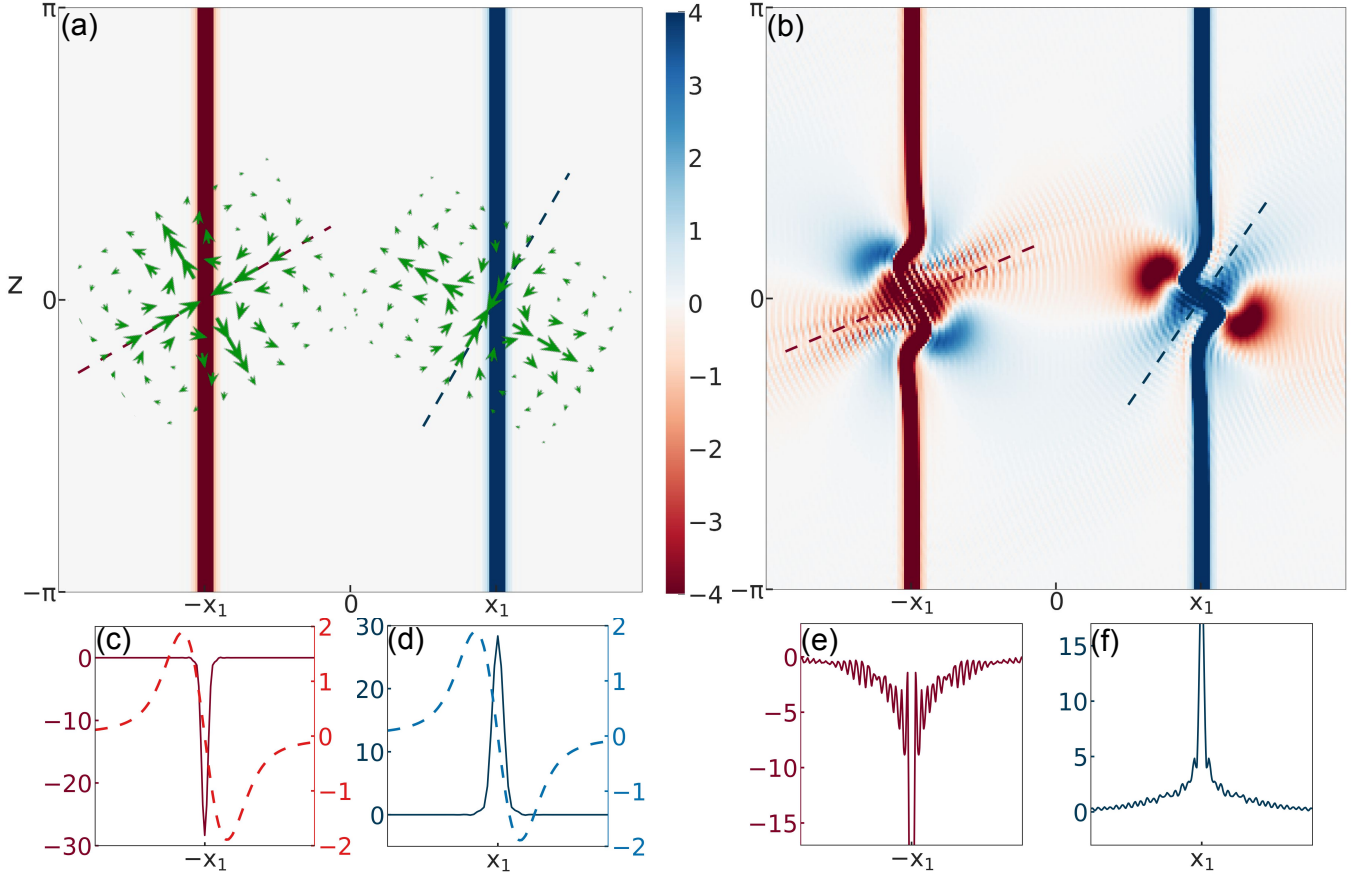


Figure 3. Pseudo-color plots of two-dimensional XZ plane cuts of ω_z for the model flow (Appendix B; Eq. (B1)) at (a) $t = 0$ and (b) $t = 0.15$ with their one-dimensional cuts (along dashed lines); the green vectors in panel (a) corresponds to the velocity field. Along the compressional directions (in panel (a), shown as a dashed red and blue lines tilted at an angles $\pi/6$ and $\pi/3$ with respect to horizontal at $x = -x_1$ and x_1 respectively) the velocity component (dashed line) and ω_z (continuous line) in panel (c) and (d) at $t = 0$. The corresponding plot for ω_z at $t = 0.15$ are shown in panels (e) and (f), respectively, showing the oscillatory behaviour with wavelength $\sim \lambda_G$. See [here](#) for an animation of the evolution of this flow to show the onset of thermalization.

able to conjecture that since the oscillations source from these sharp structures, they must be constrained to be in the same direction along which the structure is compressed. Thus the problem of knowing where in the flow the first signs of thermalization appears is reduced to an effective one-dimensional problem along very specific flow lines that generate sharp structures. This conjecture is easy to check for simpler flow geometries (such as in Fig. 3(a)). By design, it has a unique direction along with the vortex sheets are compressed as clearly seen in the streamlines in Fig. 3(a). This argument leads to the inevitable conclusion that within a short time oscillations of ω_z , with wave number k_G , should appear along the compressional directions (Fig. 3(a)).

In order to test this hypothesis, we show, in Fig. 3(b) the solution at time $t = 0.15$ of the truncated equation with the initial conditions present in panel (a). We clearly see that, consistent with our predictions, ω_z is oscillatory in the two directions of compression for the

two sheets. This hypothesis is further strengthened by performing additional simulations where the sheets are compressed along arbitrary directions (Fig. B1). In all such cases, consistent with our theory, ω_z is oscillatory in the same tilted direction along which the compression happens. The corresponding problem for the 1D Burgers equation is actually a special case of this phenomenon: In one-dimensional space, the flow is compressional and hence the oscillations, trivially seen in the velocity profile, accumulate at resonance points leading to (at early times) spatially localised structures christened *tygers* [71].

Therefore we now demonstrate, through numerical experiments with such specialized initial conditions (see Appendix B for other examples), that the onset of thermalization in the three-dimensional truncated system is essentially one-dimensional: Monochromatic oscillations arise along the compressional directions associated with fluid structures with critical velocity gradients. While

this was implicit for the generic, large-scale initial conditions which are used to solve the Galerkin-truncated Euler equation, the use of such special flows is essential to make this phenomenon evident. In more generic flows, such extreme velocity-gradient structures proliferate the flow and emerge at different times. Hence each of these structures act as independent sources of truncation waves and hence thermalization.

This observation of the precise mechanism at the heart of thermalization in 3D flows is particularly important to devise numerical strategies to arrest thermalization for the reasons discussed before. In Appendix C we suggest an algorithm, based on first decomposing the ω into local and non-local contributions and subsequently reconstructing a vorticity field by suppressing the former in a self-consistent way which preserves the small-scale intense structures while discarding the oscillations. Our preliminary results (Fig. C1(b)), albeit based on such a *static* filter (Appendix C) for the model flow, show encouraging signs that such approaches may well diminish the precursor to small-scale thermalization and allow (a) dissipative solutions and (b) extending the analyticity strip method for singularity detection to longer times than currently possible.

We acknowledge insightful remarks by M. E. Brachet and R. Kerr and important suggestions on the manuscript by R. Pandit and S. S. V. Kolluru. SSR is also indebted to U. Frisch for several discussions on this subject over many years. The simulations were performed on the ICTS clusters *Tetris*, and *Contra*. SSR acknowledges SERB-DST (India) projects MTR/2019/001553, STR/2021/000023 and CRG/2021/002766 for financial support. SSR would like to thank the Isaac Newton Institute for Mathematical Sciences for support and hospitality during the program *Mathematical aspects of turbulence: where do we stand?* (EPSRC Grant Number EP/R014604/1) when part of this work was done. The authors acknowledge the support of the DAE, Govt. of India, under project no. 12-R&D-TFR-5.10-1100 and project no. RTI4001

APPENDIX A: DIRECT NUMERICAL SIMULATIONS AND THE EVOLUTION OF THE ENERGY EQUIPARTITION SPECTRUM

We perform DNSs of the unit-density, three-dimensional, Galerkin-truncated, incompressible ($\nabla \cdot \mathbf{u} = 0$) Euler equation

$$\frac{\partial \mathbf{u}}{\partial t} = -\mathbb{P}_{k_G}[\mathbf{u} \cdot \nabla \mathbf{u} - \nabla p] \quad (\text{A1})$$

The low-pass Galerkin projector \mathbb{P}_{k_G} sets to zero all modes of the velocity field with wavenumbers larger than the prescribed Galerkin-truncation wavenumber k_G :

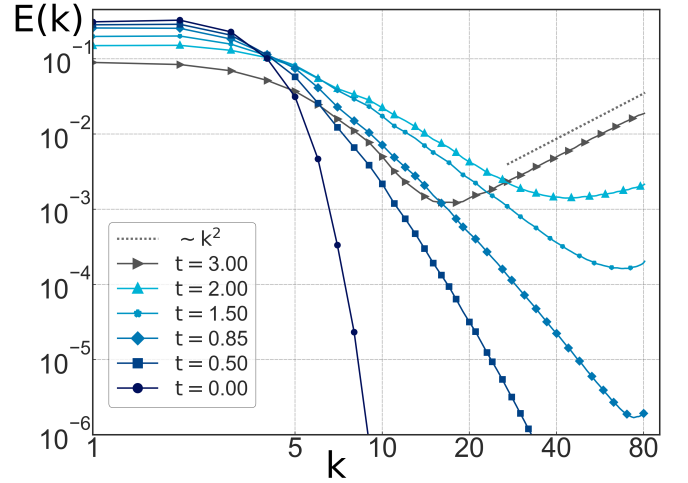


Figure A1. Loglog plots of the kinetic energy spectrum at different times from a DNS of the Galerkin-truncated Euler equation with generic, large-scale initial conditions.

$$\mathbb{P}_{k_G} \mathbf{u}(\mathbf{x}) = \sum_{|\mathbf{k}| \leq k_G} e^{i\mathbf{k} \cdot \mathbf{x}} \hat{\mathbf{u}}_{\mathbf{k}}.$$

Our DNSs use a pseudo-spectral method with a fourth-order Runge-Kutta scheme for time integration on 2π periodic domains with up to $N^3 = 512^3$ collocation points and $k_G = N/3$. Given the memory requirements for 3D visualisation of the 512^3 domains, our plots in Fig. 1 were from a 256^3 simulation. However, the 2D slices which were used in Fig. 2 were taken from the larger 512^3 data set. We have checked that our results and conclusions are consistent across simulations and choice of collocation points. We choose initial conditions (also projected on the compact Fourier domain) $E(k) \sim k^2 \exp(-k^4/k_1^4)$ to ensure that the energy is concentrated in the largest scales $k_1 \sim \mathcal{O}(1)$. Galerkin truncation ensures that the initial kinetic energy and phase space remains conserved which, coupled with the finite-dimensionality imposed by the cut-off wavenumber k_G , eventually leads to a thermalized fluid with kinetic energy equipartitioned across all Fourier modes.

Given the choice of initial conditions which confines kinetic energy at large scales, the excitement of the largest wavenumbers requires some time. In Fig. A1 we show the evolution of the kinetic energy spectrum $E(k) \equiv \frac{1}{2} \sum_{k'=k-1/2}^{k+1/2} \langle \mathbf{u}(\mathbf{k}') \cdot \mathbf{u}(\mathbf{k}') \rangle$ through representative loglog plots at various instances of time including those for which the vorticity isosurfaces have been shown in Fig. 1. Consistent with the emergence of oscillations when the largest wavenumbers are excited, we find the first signs of an equipartition spectrum $E(k) \sim k^2$ at times $t \gtrsim 0.85$. Similar evolution of the spectrum have been reported in the first study of this kind by Cichowlas *et al.* [5].

APPENDIX B: SIMULATIONS OF MODEL FLOWS

In the main text, we report results from simulation 3 of two separated vortex sheets with a localised perturbation. Such a flow configuration is generated through the following initial condition for $0 \leq x \leq \pi$:

$$u_x = \mathcal{P}_\perp \left[u_0 k_\beta (x - x_1) \exp \left(-\frac{1}{2} k_\beta^2 \left((x - x_1)^2 + y^2 + z^2 \right) \right) \right] \quad (\text{B1a})$$

$$u_y = \sqrt{2} \tanh [\gamma k_G (x - x_1)] \quad (\text{B1b})$$

$$u_z = \mathcal{P}_\perp \left[u_0 k_\beta z \exp \left(-\frac{1}{2} k_\beta^2 \left((x - x_1)^2 + y^2 + z^2 \right) \right) \right]. \quad (\text{B1c})$$

By symmetry, for $-\pi \leq x \leq 0$ the velocity field is given by $u_i(x, y, z) = (1 - 2\delta_{iz})u_i(-x, y, z)$. To ensure the incompressibility, the projection operator $\mathcal{P}_\perp[\mathbf{f}] = (1 - (\nabla_\perp^{-2})\nabla_\perp(\nabla \cdot \mathbf{f}))$ in the XZ plane ($\nabla_\perp = \{\partial_x, 0, \partial_z\}$) is applied to the x and z velocities. The disturbance here is localized at $\mathbf{x}_1 = (x_1, 0, 0)$ and $-\mathbf{x}_1$; consequently the vortex sheet is stretched for the former and compressed for the latter. The parameter γ controls the intensity of the vortex sheet and is chosen to be $1/4$ to suppress any inherent Gibbs oscillations which arise as $\gamma \rightarrow 1$. We fine-tune the extent of localisation of the perturbation through k_β which, for the results presented here, was set to 4. Finally, the flow amplitude $u_0 = 5$ sets the energy of perturbation field ($\sim 10^{-3}$ relative to that of the vortex sheet) as well as the time-scale.

In order to test the robustness of the claim and conclusions drawn from Fig. 3, we rotate the disturbance field in arbitrary directions to see if the oscillations in ω_z picks out these directions every time. In the main text we had shown (Fig. 3) results from an instance where the disturbance field u_x, u_z is rotated by $\theta = \pi/6$ from the normal of the sheet in the XZ plane for the left half of the domain with its symmetric counterpart in the right half. To further underline this point in Fig. B1 we show results from simulations where $\theta = 0$; in agreement with the conjectures in the main text, we find that ω_z is clearly oscillatory along these new directions of compression which are normal to the vortex sheet at $-\mathbf{x}_1$.

In the model flow discussed above and in the main text, the parallel vortex sheets were subject to imposed perturbations. However, to make the system more realistic, we now generalise this by immersing the two parallel vortex sheets (setting $u_x = u_z = 0$ in Eq. (B1)) in a background Taylor-Green velocity field [6] (Fig. B2(a)) and evolve this system in time by using the Galerkin-truncated Euler equation. Unlike the imposed localised perturbations before (Figs. 3 and B1), in this case it is the evolution of a large-scale background Taylor-Green flow that causes the sheets to *bend* leading to sharper gradients and eventually triggering off λ_G -wavelength oscillations in the vor-

ticity field in a manner similar to what we have already seen. In Fig. B2(a) we show a representative snapshot of this field (at time $t = 1.5$). It is immediately obvious that for the more complicated form of this flow, there are several different sources of truncation waves and directions of compression leading to a greater proliferation of thermalization *hot spots* when compared to Figs. 3(a) and B1(b) which were curated especially to isolate single directions of compression associated with each sheet.

The use of the background Taylor-Green flow has one additional advantage. In Fig. B2(b) we show the vorticity component ω_z along the middle of the domain ($z = 0$ line in Fig. B2(a)). We immediately see the absence of oscillations to the left of the two sheets. This is because in these regions the velocity gradient, along the direction of the cut S_{xx} , is negative leading to the suppression of oscillations borne out of compression.

As a final example, we simulate a vortex filament (Fig. B3(a)) in cylindrical coordinates:

$$\omega_z(r) \sim \gamma k_G \exp [-(\gamma k_G r)^2]. \quad (\text{B2})$$

Once again, this cylindrical vortex, whose thickness is determined by $\gamma = 0.25$, is immersed in a large-scale background flow which perturbs the filament. The precise form of this large-scale flow is irrelevant for the problem being studied. Not surprising the evolution of this initial condition with the truncated Burgers equations leads to oscillations which are radial with the filament at its core B3(b).

APPENDIX C: SUPPRESSING THERMALIZATION THROUGH A VORTICITY-FIELD DECOMPOSITION

Understanding how finite-dimensional equations of hydrodynamics thermalize is one aspect of this study; but perhaps the more important question relates to whether this understanding can be exploited to devise more efficient algorithms for numerical constructions of dissipative solutions of the Euler equations and indeed conjectures for finite-time blow-up through methods such as the analyticity strip [59, 73, 74].

Operationally this would involve suppressing the oscillations which trigger the flow to thermalize—making analyticity strip approaches to singularity detection impractical [74]—and ensure conservation of energy and thus the lack of dissipative solutions. From our DNSs it seems that a useful starting point would be a suitable filtering of the strain field (Fig. 2) to remove the oscillatory structures.

To achieve this we adapt the method developed by Hamlington *et al.* [84] to decompose the strain field into a local and non-local (background) contribution. This

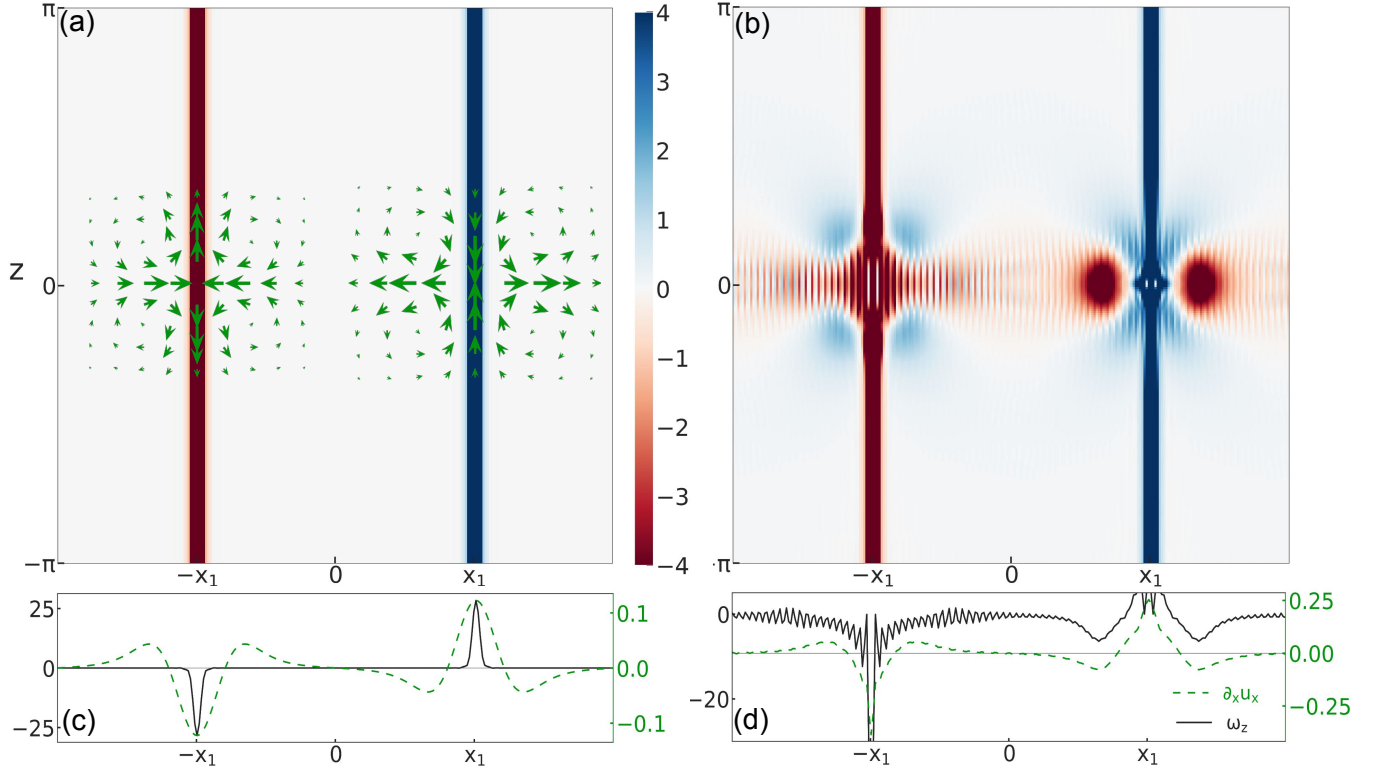


Figure B1. Pseudo-color plots of two-dimensional XZ plane cuts of ω_z for the model flow (Eq. (B1)) at (a) $t = 0$ and (b) $t = 0.15$ with their one-dimensional cuts ($z = 0$) and those of the velocity gradient $\partial_x u_x$ at the corresponding times in panels (c) and (d), respectively. The initial profiles (panels (a) and (c)) are devoid of the λ_G wavelength oscillations which show up at later times along the directions of compression indicated by the velocity vectors (green arrows) in panel (a). These oscillations are conspicuous, as clearly seen in panel (d) in regions of positive strain: $\partial_x u_x \geq 0$.

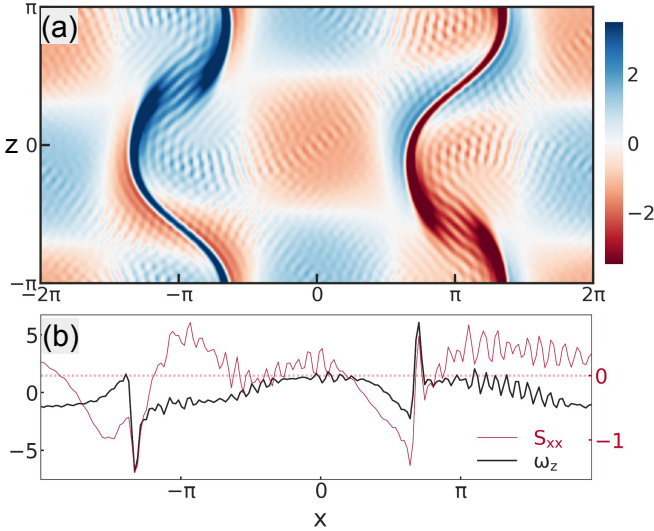


Figure B2. (a) A pseudo-color plot of the two-dimensional XZ plane cut of ω_z for a pair of vortex sheets advected by a Taylor-Green flow at time $t = 1.3$. (b) The one-dimensional cut of ω_z and the strain component S_{xx} along the thick, dashed horizontal line of panel (a) shows the strong correlation between the thermalization-inducing oscillations and positive values of S_{xx} .

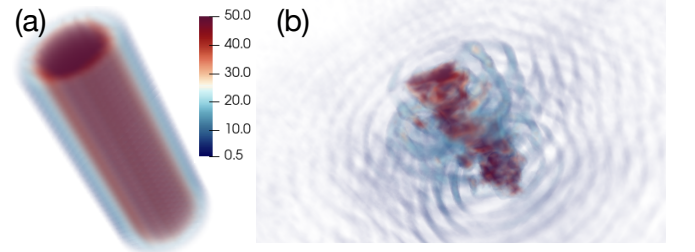


Figure B3. Pseudo-color plots of ω_z at (a) $t = 0$ and (b) $t = 0.8$; the axis of the vortex filament is aligned along the z direction.

is trivially done for the vorticity field in Fourier space via

$$\hat{\omega}^{(NL)}(\mathbf{k}) = f(kR)\hat{\omega}(\mathbf{k}) \quad (C1)$$

$$\hat{\omega}^{(L)}(\mathbf{k}) = \hat{\omega} - \hat{\omega}^{(NL)} \quad (C2)$$

where the *hat* denotes Fourier space, the subscripts L and NL stand for the “local” and “non-local”, respectively, $k = |\mathbf{k}|$ and the filter

$$f(kR) = \frac{3(\sin(kR) - kR \cos(kR))}{(kR)^3} \quad (C3)$$

is the Fourier transform of the three-dimensional complementary Heaviside function in spherical co-ordinates. Such a filter, by definition, ensures that the function on which it acts—namely the vorticity field in this case—is *smoothened* by averaging out over a sphere of radius $R = \lambda_G$. Evidently, the local contribution ω^L alone contains all the oscillations and hence the “reconstructed” field $\omega^* \equiv \omega^{NL}$ with ω^L suppressed should be free of oscillations. Hence such a *dynamic* filtering technique, namely, solving the truncated 3D Euler by recovering ω^* and using this field to evolve at every time-step, should yield a non-thermalizing, dissipative flow.

However, such an approach has the disadvantage that along with the oscillations, the small-scale, intense vortical structures are lost as well. We therefore adapt this idea of decomposing the field in a way which preserves the small-scale structures as far as possible and yet suppress the oscillatory triggers of thermalization. Thus, we propose:

$$\omega^*(\mathbf{x}) = \omega^{(NL)}(\mathbf{x}) + \Gamma_{2m}(\mathbf{x})\omega^{(L)}(\mathbf{x}) \quad (C4)$$

$$\Gamma_{2m}(\mathbf{x}) := \text{erf} \left[\frac{|\omega|^{2m}}{\|\omega\|_{2m}^{2m}} \right]. \quad (C5)$$

The additional regularisation parameter Γ_{2m} allows us to capture the essential, intense local vortical regions while still filtering out the oscillations in the flow. The L_{2m} norm used in the definition of Γ_{2m} further controls threshold level of that vortical regions we want to retain in the reconstructed field.

While this method needs to be refined and rigorously examined in future studies for generic flow fields, we provide results from preliminary tests conducted on the model flow defined by Eq. (B1). In Fig. C1(a) we show the reconstructed vorticity field at $t = 0.15$ for $m = 4$, corresponding to the snapshot shown in Fig. B1(b). A visual comparison of the two vorticity fields show that our reconstruction strategy indeed leads to a significant reduction in the oscillations while still preserving the intense structures, namely the vortical sheets in this case. This is quantified, in Fig. C1(b), by comparing the z -component of the vorticity along the x -axis ($z = 0$) in the middle of the domain for the truncated (ω_z) and reconstructed fields (ω_z^*). We clearly see that the oscillations responsible for thermalization, seen in ω_z more or less vanish on reconstruction as seen in the plot of (ω_z^*). Furthermore our use of the regularisation parameter Γ_{2m} does preserve fully the intense structure in the form of vortex sheets as seen by the near overlap of ω_z and ω_z^* at $-x_1$ and x_1 .

While Fig. C1(b) seems to underline the success of this strategy—at least for such a curated flow—the illustrative flow field shown in panel (a) still retains some traces of the oscillations. There are at least two reasons why this is so. Firstly in our tests we have not filtered and reconstructed the field at every time step but, as a proof of

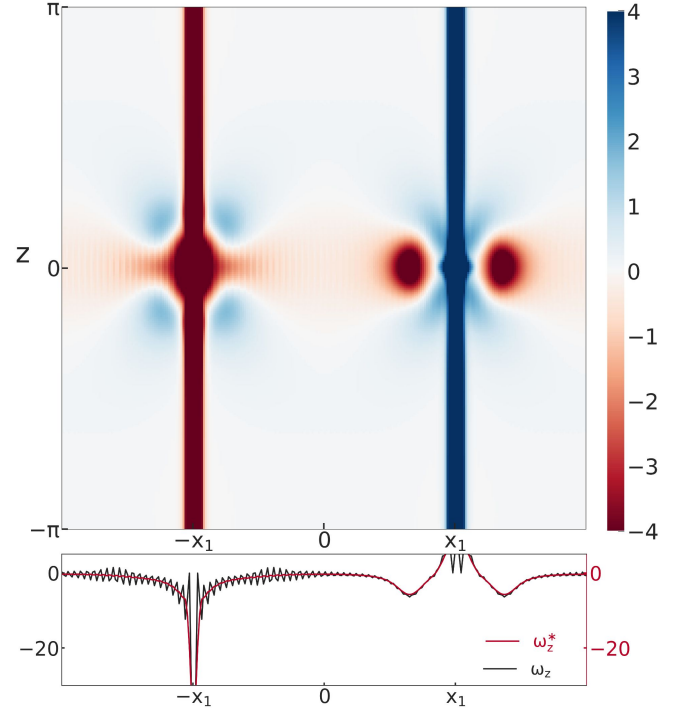


Figure C1. (a) Pseudo-color plot of the two-dimensional XZ plane cut of the reconstructed vorticity field ω_z^* for the model flow (Eq. (B1)) at $t = 0.15$. A comparison with the corresponding figure (Fig. 3(b)) of truncated simulation shows a significant suppression of the oscillations. This is quantified in (b) plots of the one-dimensional cuts (along $z = 0$) ω_z (same as in Fig. 3(d)) and ω_z^* , as a function of x , along the center of the domain.

principle now, used this as a *static* filter and reconstruction at $t = 0.15$. A dynamic filter, as discussed above, is essential and, perhaps, the frequency—the time-intervals between successive filtering—with which the filter should be applied needs further investigation. The latter may well be a delicate point as shown in Ref. [77] for Fourier space purging in the 1D Burgers equation.

Secondly, our preliminary explorations with different sharpness of the regularisation parameter Γ_{2m} , shows that this, not surprisingly, is critically important for more effective suppression of thermalization hotspots, especially in the vicinity of flow structures with intense gradients. This will become crucial when such strategies are investigated systematically in generic 3D flows.

* sugan.murugan@icts.res.in

† samriddhisankarray@gmail.com

- [1] E. Hopf, *Journal of Rational Mechanics and Analysis* **1**, 87 (1952).
- [2] T. D. Lee and C. N. Yang, *Phys. Rev.* **87**, 410 (1952).
- [3] R. H. Kraichnan, *The Physics of Fluids* **10**, 1417 (1967).
- [4] R. H. Kraichnan, *Journal of Fluid Mechanics* **59**, 745

- (1973).
- [5] C. Cichowlas and M.-E. Brachet, *Fluid Dynamics Research* **36**, 239 (2005).
 - [6] C. Cichowlas, P. Bonaïti, F. Debbasch, and M. Brachet, *Phys. Rev. Lett.* **95**, 264502 (2005).
 - [7] G. Krstulovic and M.-E. Brachet, *Physica D: Nonlinear Phenomena* **237**, 2015 (2008).
 - [8] E. Hopf, *Comm. Pure Appl. Math.* **3**, 201 (1950).
 - [9] S. D. Murugan, D. Kumar, S. Bhattacharjee, and S. S. Ray, *Phys. Rev. Lett.* **127**, 124501 (2021).
 - [10] C. Rampf, U. Frisch, and O. Hahn, *arXiv e-prints*, [arXiv:2207.12416](https://arxiv.org/abs/2207.12416) (2022).
 - [11] J. Bec and K. Khanin, *Phys. Rep.* **447**, 1 (2007).
 - [12] Rose, H. A. and Sulem, P. L., *J. Phys. France* **39**, 441 (1978).
 - [13] S. A. Orszag, *Journal of Fluid Mechanics* **41**, 363 (1970).
 - [14] U. Frisch, *Turbulence: The Legacy of A. N. Kolmogorov* (Cambridge University Press, Cambridge, The United Kingdom, 1995).
 - [15] R. H. Kraichnan, *Journal of Fluid Mechanics* **5**, 497 (1959).
 - [16] A. N. Kolmogorov, V. Levin, J. C. R. Hunt, O. M. Phillips, and D. Williams, *Proceedings of the Royal Society of London. Series A: Mathematical and Physical Sciences* **434**, 9 (1991).
 - [17] V. S. L'vov, A. Pomyalov, and I. Procaccia, *Phys. Rev. Lett.* **89**, 064501 (2002).
 - [18] U. Frisch, A. Pomyalov, I. Procaccia, and S. S. Ray, *Phys. Rev. Lett.* **108**, 074501 (2012).
 - [19] A. S. Lanotte, R. Benzi, S. K. Malapaka, F. Toschi, and L. Biferale, *Phys. Rev. Lett.* **115**, 264502 (2015).
 - [20] A. S. Lanotte, S. K. Malapaka, and L. Biferale, *Eur. Phys. J. E* **39**, 49 (2016).
 - [21] M. Buziccotti, L. Biferale, U. Frisch, and S. S. Ray, *Phys. Rev. E* **93**, 033109 (2016).
 - [22] M. Buziccotti, A. Bhatnagar, L. Biferale, A. S. Lanotte, and S. S. Ray, *New J. Phys.* **18**, 113047 (2016).
 - [23] S. S. Ray, *Phys. Rev. Fluids* **3**, 072601 (2018).
 - [24] R. Tom and S. S. Ray, *Europhys. Lett.* **120**, 34002 (2017).
 - [25] J. R. Picardo, A. Bhatnagar, and S. S. Ray, *Phys. Rev. Fluids* **5**, 042601 (2020).
 - [26] U. Frisch, S. Kurien, R. Pandit, W. Pauls, S. S. Ray, A. Wirth, and J.-Z. Zhu, *Phys. Rev. Lett.* **101**, 144501 (2008).
 - [27] U. Frisch, S. S. Ray, G. Sahoo, D. Banerjee, and R. Pandit, *Phys. Rev. Lett.* **110**, 064501 (2013).
 - [28] D. Banerjee and S. S. Ray, *Phys. Rev. E* **90**, 041001 (2014).
 - [29] D. Bandak, N. Goldenfeld, A. A. Mailybaev, and G. Eyink, *Phys. Rev. E* **105**, 065113 (2022).
 - [30] J.-D. Fournier and U. Frisch, *Phys. Rev. A* **17**, 747 (1978).
 - [31] A. Celani, S. Musacchio, and D. Vincenzi, *Phys. Rev. Lett.* **104**, 184506 (2010).
 - [32] J. Leray and R. Terrell, *arXiv e-prints*, [arXiv:1604.02484](https://arxiv.org/abs/1604.02484) (2016), [arXiv:1604.02484 \[math.HO\]](https://arxiv.org/abs/1604.02484).
 - [33] L. Onsager, *Nuovo Cim* **6**, 279 (1949).
 - [34] J. D. Gibbon, *Physica D: Nonlinear Phenomena Euler Equations: 250 Years On*, **237**, 1894 (2008).
 - [35] J. D. Gibbon, M. Bustamante, and R. M. Kerr, *Nonlinearity* **21**, T123 (2008).
 - [36] U. Frisch, T. Matsumoto, and J. Bec, *Journal of Statistical Physics* **113** (2002), [10.1023/A:1027308602344](https://doi.org/10.1023/A:1027308602344).
 - [37] M. E. Brachet, D. I. Meiron, S. A. Orszag, B. G. Nickel, R. H. Morf, and U. Frisch, *Journal of Fluid Mechanics* **130**, 411 (1983).
 - [38] M. E. Brachet, M. Meneguzzi, A. Vincent, H. Politano, and P. L. Sulem, *Physics of Fluids A: Fluid Dynamics* **4**, 2845 (1992).
 - [39] O. N. Boratav, R. B. Pelz, and N. J. Zabusky, *Physics of Fluids A: Fluid Dynamics* **4**, 581 (1992).
 - [40] R. M. Kerr, *Physics of Fluids A: Fluid Dynamics* **5**, 1725 (1993).
 - [41] M. J. Shelley, D. I. Meiron, and S. A. Orszag, *J. Fluid Mech.* **246**, 613 (1993).
 - [42] O. N. Boratav and R. B. Pelz, *Physics of Fluids* **6**, 2757 (1994).
 - [43] R. M. Kerr, *Physics of Fluids* **17**, 075103 (2005).
 - [44] R. Pelz and K. Ohkitani, *Fluid Dynamics Research* **36**, 193 (2005).
 - [45] T. Y. Hou and R. Li, *J Nonlinear Sci* **16**, 639 (2006).
 - [46] G. Luo and T. Y. Hou, *Proc. Natl. Acad. Sci. U.S.A.* **111**, 12968 (2014).
 - [47] D. W. Moore, *Proceedings of the Royal Society of London. Series A, Mathematical and Physical Sciences* **365**, 105 (1979).
 - [48] R. H. Morf, S. A. Orszag, and U. Frisch, *Phys. Rev. Lett.* **44**, 572 (1980).
 - [49] R. B. Pelz and Y. Gulak, *Phys. Rev. Lett.* **79**, 4998 (1997).
 - [50] Y. Gulak and R. Pelz, *Fluid Dyn. Res.* **36**, 211 (2005).
 - [51] A. J. Chorin, *Commun.Math. Phys.* **83**, 517 (1982).
 - [52] E. D. Siggia, *The Physics of Fluids* **28**, 794 (1985).
 - [53] A. Pumir and E. Siggia, *Physics of Fluids A: Fluid Dynamics* **2**, 220 (1990).
 - [54] J. B. Bell and D. L. Marcus, *Commun.Math. Phys.* **147**, 371 (1992).
 - [55] R. B. Pelz, *Phys. Rev. E* **55**, 1617 (1997).
 - [56] R. Grauer and T. C. Sideris, *Phys. Rev. Lett.* **67**, 3511 (1991).
 - [57] R. Grauer, C. Marliani, and K. Germaschewski, *Phys. Rev. Lett.* **80**, 4177 (1998).
 - [58] P. Orlandi and G. F. Carnevale, *Physics of Fluids* **19**, 057106 (2007).
 - [59] S. S. V. Kolluru, P. Sharma, and R. Pandit, *Phys. Rev. E* **105**, 065107 (2022).
 - [60] J. T. Beale, T. Kato, and A. Majda, *Commun.Math. Phys.* **94**, 61 (1984).
 - [61] G. Ponce, *Communications in Mathematical Physics* **98**, 349 (1985).
 - [62] P. Constantin, C. Fefferman, and A. J. Majda, *Commun Part Diff Eq* **21** (1996).
 - [63] P. Constantin, *Physica D: Nonlinear Phenomena* **237**, 1926 (2008).
 - [64] G. L. Eyink, *Physica D: Nonlinear Phenomena Euler Equations: 250 Years On*, **237**, 1956 (2008).
 - [65] D. Chae, *Communications on Pure and Applied Mathematics* **60**, 597 (2007).
 - [66] J. Deng, T. Y. Hou, and X. Yu, *Communications in Partial Differential Equations* **30**, 225 (2005).
 - [67] J. Deng, T. Y. Hou, and X. Yu, *Communications in Partial Differential Equations* **31**, 293 (2006).
 - [68] T. Y. Hou and R. Li, *Physica D: Nonlinear Phenomena Euler Equations: 250 Years On*, **237**, 1937 (2008).
 - [69] C. Canuto, M. Y. Hussaini, A. Quarteroni, and T. A. Zang, Jr, *Spectral Methods in Fluid Dynamics* (Springer Science & Business Media, 2012).
 - [70] R. J. Leveque, *Numerical Methods for Conservation Laws*

- (Birkhäuser Verlag, 1990).
- [71] S. S. Ray, U. Frisch, S. Nazarenko, and T. Matsumoto, *Phys. Rev. E* **84**, 016301 (2011).
 - [72] D. Venkataraman and S. S. Ray, *Proceedings of the Royal Society A: Mathematical, Physical and Engineering Sciences* **473**, 20160585 (2017).
 - [73] C. Sulem, P. L. Sulem, and H. Frisch, *Journal of Computational Physics* **50**, 138 (1983).
 - [74] M. Bustamante and M.-E. Brachet, *Physical review. E, Statistical, nonlinear, and soft matter physics* **86**, 066302 (2012).
 - [75] R. M. Pereira, R. Nguyen van yen, M. Farge, and K. Schneider, *Phys. Rev. E* **87**, 033017 (2013).
 - [76] M. Farge, N. Okamoto, K. Schneider, and K. Yoshimatsu, *Phys. Rev. E* **96**, 063119 (2017).
 - [77] S. D. Murugan, U. Frisch, S. Nazarenko, N. Besse, and S. S. Ray, *Phys. Rev. Research* **2**, 033202 (2020).
 - [78] R. M. Pereira, N. N. van yen, K. Schneider, and M. Farge, *arXiv:2111.04863 [physics]* (2021).
 - [79] W. J. T. Bos and J.-P. Bertoglio, *Physics of Fluids* **18**, 071701 (2006).
 - [80] G. Krstulovic, P. D. Mininni, M. E. Brachet, and A. Pouquet, *Phys. Rev. E* **79**, 056304 (2009).
 - [81] A. J. Majda and I. Timofeyev, *Proceedings of the National Academy of Sciences* **97**, 12413 (2000), <https://www.pnas.org/doi/pdf/10.1073/pnas.230433997>.
 - [82] P. Clark di Leoni, P. Mininni, and M.-E. Brachet, *Physical Review Fluids* **3** (2017), 10.1103/PhysRevFluids.3.014603.
 - [83] A. J. Chorin, *Communications on Pure and Applied Mathematics* **39**, S47 (1986).
 - [84] P. E. Hamlington, J. Schumacher, and W. J. A. Dahm, *Phys. Rev. E* **77**, 026303 (2008).